Ultrasound in Medicine & Biology 50 (2024) 661–670

Contents lists available at ScienceDirect

Ultrasound in Medicine & Biology

journal homepage: www.elsevier.com/locate/ultrasmedbio

Original Contribution

Mitral Valve Segmentation and Tracking from Transthoracic Echocardiography Using Deep Learning

Sigurd Vangen Wifstad [a,*], Henrik Agerup Kildahl [a,b], Bjørnar Grenne [a,b], Espen Holte [a,b], Ståle Wågen Hauge [a,b,c], Sigbjørn Sæbø [a,b], Desalew Mekonnen [d], Berhanu Nega [d], Rune Haaverstad [c], Mette-Elise Estensen [e], Håvard Dalen [a,b], Lasse Lovstakken [a]

[a] Department of Circulation and Medical Imaging, Norwegian University of Science and Technology, Trondheim, Norway
[b] Clinic of Cardiology, St. Olav's Hospital, Trondheim University Hospital, Trondheim, Norway
[c] Haukeland University Hospital, Bergen, Norway
[d] Tikur Anbessa Specialized Hospital, Addis Ababa, Ethiopia
[e] Oslo University Hospital, Oslo, Norway

ARTICLE INFO

Keywords:
Transthoracic echocardiography
Valvular heart disease
Mitral valve
Deep learning
Attention gates
Medical image segmentation
Tracking
Time series
Quantitative assessment

Objective: Valvular heart diseases (VHDs) pose a significant public health burden, and deciding the best treatment strategy necessitates accurate assessment of heart valve function. Transthoracic echocardiography (TTE) is the key modality to evaluate VHDs, but the lack of standardized quantitative measurements leads to subjective and time-consuming assessments. We aimed to use deep learning to automate the extraction of mitral valve (MV) leaflets and annular hinge points from echocardiograms of the MV, improving standardization and reducing workload in quantitative assessment of MV disease.

Methods: We annotated the MV leaflets and annulus points in 2931 images from 127 patients. We propose an approach for segmenting the annotated features using Attention UNet with deep supervision and weight scheduling of the attention coefficients to enforce saliency surrounding the MV. The derived segmentation masks were used to extract quantitative biomarkers for specific MV leaflet scallops throughout the heart cycle.

Results: Evaluation performance was summarized using a Dice score of 0.63 ± 0.14, annulus error of 3.64 ± 2.53 and leaflet angle error of 8.7 ± 8.3°. Leveraging Attention UNet with deep supervision robustness of clinically relevant metrics was improved compared with UNet, reducing standard deviations by 2.7° (angle error) and 0.73 mm (annulus error). We correctly identified cases of MV prolapse, cases of stenosis and healthy references from a clinical material using the derived biomarkers.

Conclusion: Robust deep learning segmentation and tracking of MV morphology and motion is possible by leveraging attention gates and deep supervision, and holds promise for enhancing VHD diagnosis and treatment monitoring.

Introduction

Valvular heart diseases (VHDs) constitute a class of diseases that affect the function of the heart valves, including obstruction of blood flow (valve stenosis) and leakage of blood (valve regurgitation), representing an increasing burden to the public health system [1]. Transthoracic echocardiography (TTE) is the primary modality used to assess VHDs. Current recommendations [2,3] emphasize an integrative approach of quantitative and indirect measurements limited to blood flow measurements (Doppler) and dimensions and volumes of heart chambers. This approach is time-consuming, dependent on the clinician's experience and skill and vulnerable to significant inter-observer variability [4–6].

Quantitative predictors for MV morphology and motion based on leaflet angle and tenting area have previously been proposed [7–9]. Currently, direct quantitative measurements require tedious manual annotation of several images for each recording, which is rarely considered feasible. Automating direct quantification of VHDs could facilitate standardization and reduce workload in the clinic.

Moreover, standardized measurements of leaflet motion could be beneficial for regular patient follow-up to monitor the disease progression of the valve condition according to a given treatment. Tracking the MV through the heart cycle could also unveil relevant information about cardiac function and filling pressures. By further enabling the extraction of these measurements in large databases, it may be possible to improve

* Corresponding author. Department of Circulation and Imaging, Norwegian University of Science and Technology (NTNU), Prinsesse Kristinas Gate 3, 7030, Trondheim, Norway.
E-mail address: sigurd.v.wifstad@ntnu.no (S.V. Wifstad).

https://doi.org/10.1016/j.ultrasmedbio.2023.12.023
Received 29 August 2023; Revised 27 November 2023; Accepted 24 December 2023

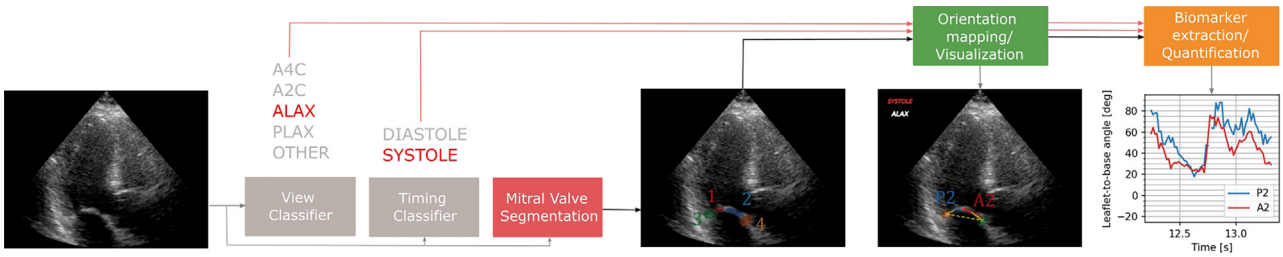

Figure 1. Application pipeline overview. Mitral valve leaflets and annulus hinge points are segmented from transthoracic echocardiograms. The relevant leaflet scallop labels (P2, central posterior scallop; A2, central anterior scallop) are assigned to the segmentation classes according to the predicted view. Biomarkers for each leaflet are computed from the segmentation output sequence. The timing prediction extracts biomarkers at relevant phases in the cardiac cycle.

the diagnostic and prognostic value of echocardiographic markers of VHDs and cardiac function.

Measurement of mitral valve (MV) morphology and motion has previously been achieved with various unsupervised approaches [10–13]. However, these approaches are susceptible to motion artifacts from surrounding tissue and poor performance for poor-quality images. In recent years, convolutional neural networks (CNNs) have shown great promise in medical image segmentation. CNNs have also been successfully applied to segmentation of the MV leaflets from TTE images. Costa et al. [14] trained a UNet to segment the MV leaflets in children with rheumatic valve disease, with promising results. In addition to segmentation, classification of VHDs from TTE images using deep learning has also recently been proposed [15]. Moreover, several studies [16–19] have explored three-dimensional segmentation and tracking of the MV leaflets and annulus in transesophageal echocardiography (TEE). Three-dimensional TTE is non-invasive but currently hampered by a lower frame rate and poorer image quality, which makes segmentation and tracking of the MV more challenging.

The UNet architecture is often used for medical image segmentation as it has been proven to provide robust segmentation results across a wide range of tasks. However, segmentation of the MV from echocardiograms poses extra challenges for learning spatial features. The MV leaflets are dynamic, thin structures with varying profiles throughout the cardiac cycle, which are influenced by patient-specific image quality,

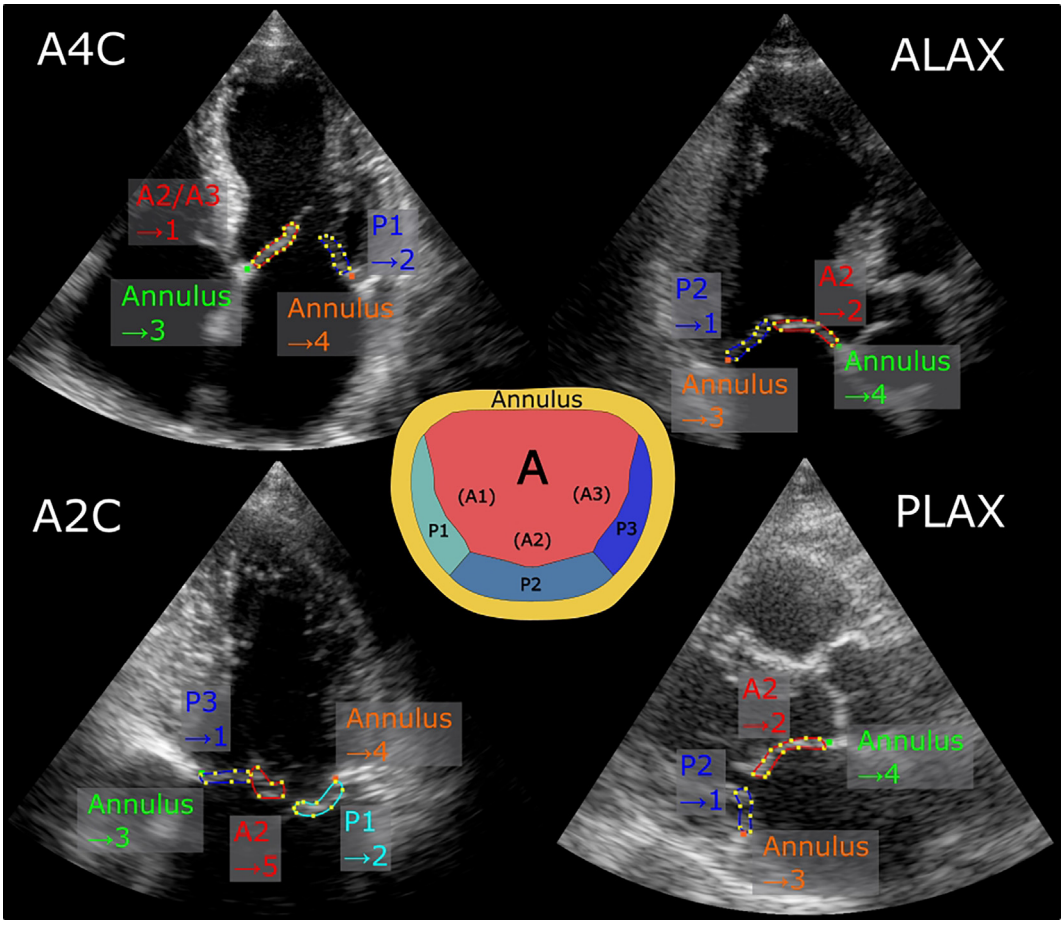

Figure 2. Four images with different cardiac views (A4C, A2C, ALAX, PLAX) annotated using AnnotationWeb. The leaflets and annulus points were annotated as separate classes according to the mitral valve anatomy, depicted by the center illustration (A, anterior; P, posterior; 1, anterolateral; 2, central; 3, posteromedial). To simplify the complexity of the learning task across different views, the classes were mapped to values 1–5 according to left–right orientation labeling, as indicated by the arrows. Five to ten key frames at different points in the cardiac cycle were annotated for each recording. A5C views were grouped under the same category as A4C views. ALAX, apical long axis; PLAX, parasternal long axis.

potential obstruction in the view and the possibility of misidentification with other visible cardiac structures, such as other valves and cardiac walls. Thus, robust tracking of the MV over time is a significant challenge.

First, we aimed to automate the extraction of key measurements of the MV leaflets and annular hinge points from TTE images in apical two-, four- and five-chamber (A2C, A4C, A5C) and apical and parasternal long-axis (ALAX, PLAX) views. Second, we aimed to evaluate the robustness of MV segmentation for different deep learning architectures. The overarching goal was to enhance standardization and reduce operator bias and workload in quantitative assessment of the MV pathology.

The main contribution of this work includes a deep learning-based approach for segmenting the MV, using attention gates and deep supervision (DS) for improved robustness. We also describe the automatic extraction of clinical biomarkers for MV motion and morphology and how they relate to VHD.

Methods

Application pipeline

A MV segmentation network was combined with cardiac event timing (systole/diastole) and imaging view classifiers to produce automated quantitative measurements for specific leaflet scallops at relevant time points. The pipeline is illustrated in Figure 1. For each of the identified scallops, we extracted quantitative biomarkers (leaflet angle, leaflet tenting area and leaflet angular velocity), which were used for tracking of MV motion and morphology and identification of MV disease. For imaging view and cardiac timing classification, we used neural networks from previous work in our research group [20,21].

Data sets

The data set used for training and evaluation consisted of transthoracic echocardiograms from 78 patients with MV disease acquired at St. Olav's Hospital, Trondheim, Norway, between 2015 and 2021, and 49 patients with rheumatic MV disease acquired at Tinkur Anbessa Specialized Hospital in Addis Ababa, Ethiopia, between 2017 and 2019. The regional medical and health research committees approved the use of all image data in this work. The data set consisted of B-mode echocardiograms acquired using GE Vivid E9/E95 scanners (GE Vingmed Ultrasound AS, Horten, Norway), with the primary standard views for VHD assessment (A2C, A4C, A5C, ALAX, PLAX). A total of 2931 images from 438 recordings from 127 patients were annotated. The data set had a representative distribution of image quality and consisted of both high- and poor-quality images. About 5–10 image frames were annotated in each recording. The image frames were chosen manually by the annotators to capture the MV range of motion, including end-systole and end-diastole frames and the MV opening phase. The anterior and posterior valve leaflets and the annulus hinge points were annotated using AnnotationWeb [22], as illustrated in Figure 2. Experienced clinicians performed the annotations.

Attention UNet with deep supervision

To mitigate false-positive segmentation of irrelevant features, focus should be placed on the salient region around the MV during training. We used the Attention UNet [23] to enhance focus on the region of interest. This architecture introduces attention gates that leverage the multiplication of saliency maps with the image tensors, encouraging the network to segment only relevant regions. We applied DS on the attention coefficients to enforce saliency around

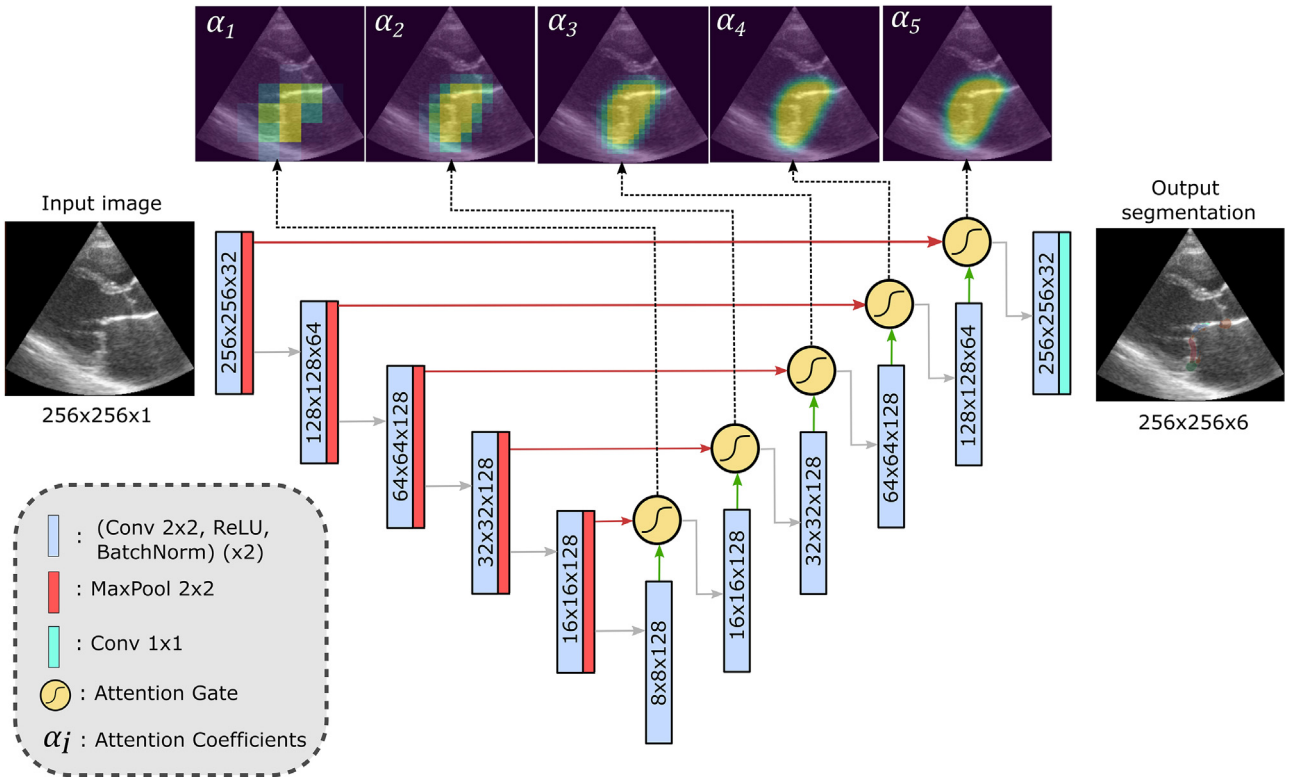

Figure 3. Model architecture: Attention UNet with deep supervision. The network outputs six segmentation class labels (background, three leaflets, two annulus hinge points) for a given image. In addition, attention coefficient maps α_i are taken as outputs for early-stage deep supervision. The network is trained to output saliency maps surrounding the mitral valve in this stage. Hence α_i are primed to focus on the correct spatial features in the image before the segmentation task is gradually introduced and eventually dominates the learning task.

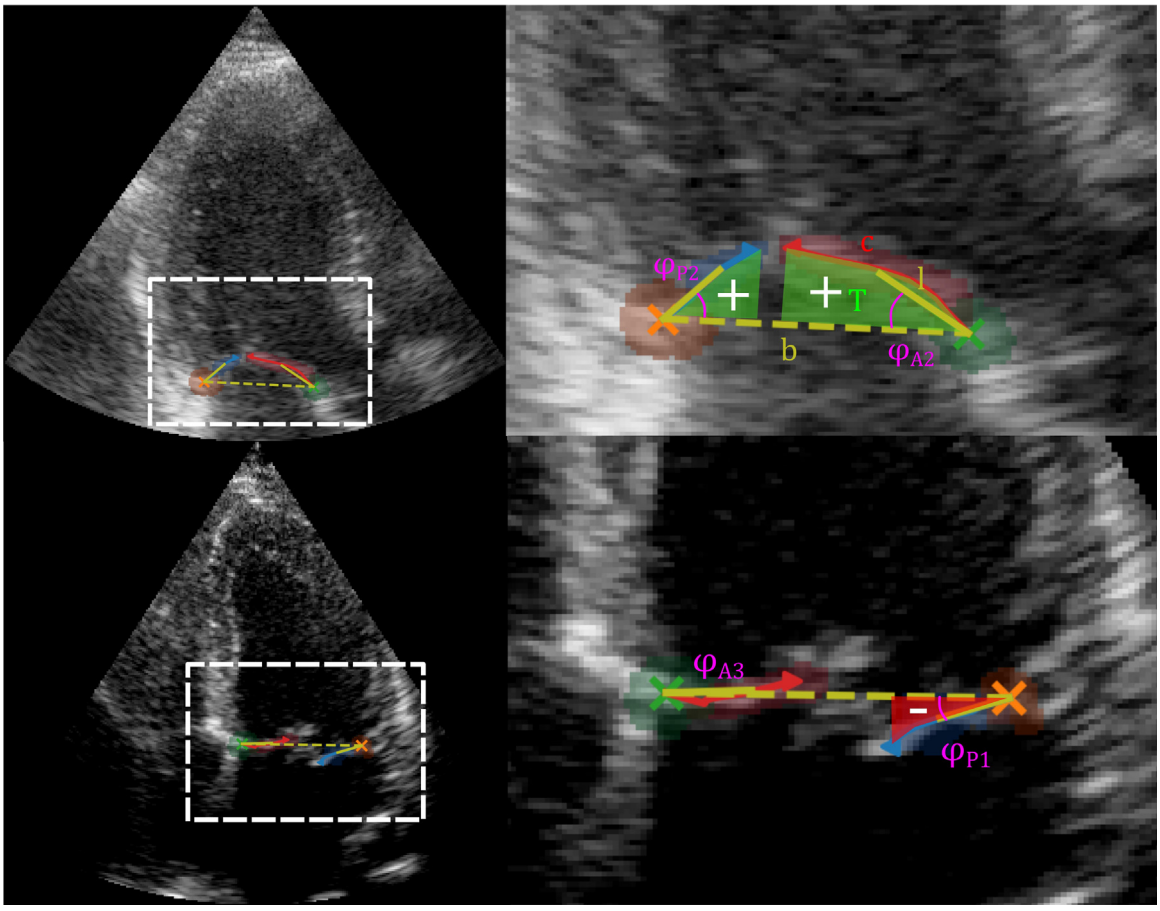

Figure 4. Segmentation examples with an illustration of biomarker extraction. Leaflet vectors l (*solid yellow lines*) are computed from the segmentation output centroid of the leaflet and the corresponding annulus hinge point (*green and orange cross*). The annular plane vector ***b*** (*dashed yellow line*) is computed between the two hinge points. For each identified leaflet scallop (A, anterior; P, posterior; 1, anterolateral; 2, central; 3, posteromedial) we compute the leaflet opening angle φ, the leaflet angular momentum $d\varphi/dt$ and the signed tenting area T between the leaflet center curves c (*red and blue curves*) and b.

Table 1
Performance comparison of different models

	70%/30% Train/test split			30%/70% Train/Test Split		
Metric	UNet	Attention UNet	Attention UNet + DS	UNet	Attention UNet	Attention UNet + DS
Dice score	**0.64 ± 0.15**	0.63 ± 0.16	0.63 ± 0.14	0.36 ± 0.22	0.43 ± 0.23	**0.46 ± 0.19**
Precision	**0.69 ± 0.17**	0.64 ± 0.17	0.65 ± 0.17	0.35 ± 0.21	**0.42 ± 0.22**	0.39 ± 0.18
Recall	0.62 ± 0.17	0.64 ± 0.19	**0.64 ± 0.17**	0.41 ± 0.28	0.48 ± 0.28	**0.61 ± 0.26**
Hausdorff (mm)	**12.91 ± 12.78**	21.82 ± 19.64	14.17 ± 11.88	37.08 ± 20.16	38.26 ± 20.12	**24.34 ± 13.66**
Annulus error (mm)	3.64 ± 3.36	4.85 ± 5.53	3.64 ± 2.53	8.21 ± 9.73	9.50 ± 10.65	**6.93 ± 7.25**
Spline error (mm)	3.57 ± 1.92	3.74 ± 2.25	**3.11 ± 1.06**	7.48 ± 3.63	6.83 ± 4.42	**5.34 ± 3.01**
Angle error (°)	9.56 ± 10.99	12.67 ± 17.01	**8.67 ± 8.32**	23.50 ± 24.42	24.65 ± 27.99	**18.35 ± 16.85**
TCS	0.85 ± 0.20	0.79 ± 0.19	**0.93 ± 0.10**	0.60 ± 0.25	0.59 ± 0.25	**0.92 ± 0.13**

Significant improvements ($p < 0.05$) are emphasized in boldface type. Dice score, precision and recall are evaluated only for the leaflet classes. The TCS is the fraction of frames in a recording that pass the automatic temporal consistency evaluation. Spline error is computed as the mean absolute error of estimated center curve splines from the ground truth annotations relative to the predictions. TCS, temporal consistency score

the MV. We achieved this by computing segmentation loss on the output and attention maps, where the latter was optimized to enforce saliency heatmaps around the MV. The model architecture is illustrated in Figure 3.

Because the MV is small compared with the image dimensions, the training data had a high class imbalance. To mitigate the class imbalance, we used a balanced cross-entropy loss. The segmentation loss function $\mathscr{L}_{\text{seg}}$ computed between the ground truth tensor y and the predicted tensor $\hat{y}$ is defined as

$$\mathscr{L}_{\text{seg}} = -\beta y \log(\hat{y}) - (1-\beta)(1-y)\log(1-\hat{y}) \quad (1)$$

where β is the mean value of each channel in the tensor y.

The total loss function L was computed as a weighted sum of all of the loss functions according to

$$\mathscr{L} = \lambda(n)\mathscr{L}_{\text{seg}} + \frac{1-\lambda(n)}{5}\sum_{i=1}^{5}\mathscr{L}_{\alpha}^{(i)} \quad (2)$$

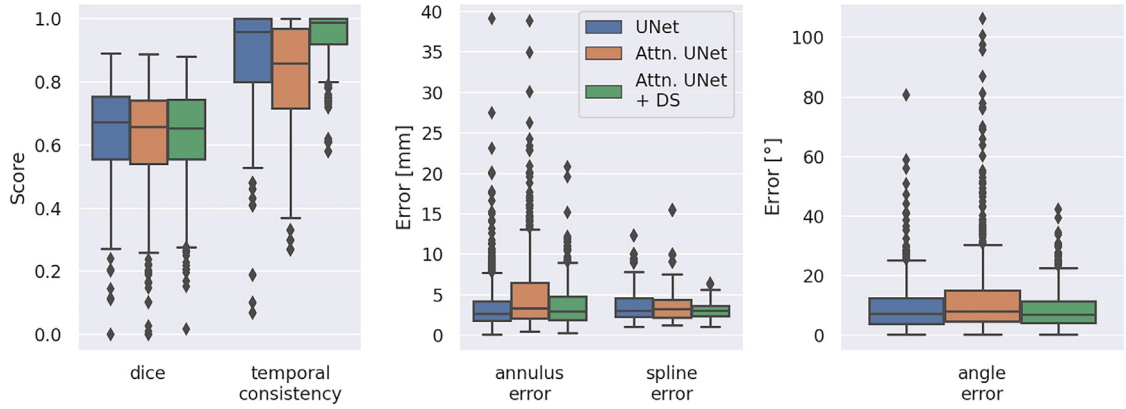

Figure 5. Boxplot of central test results for the different models (70%/30% train/test split). Metrics were computed as explained in Table 1. We can observe notable outlier reduction for Attention UNet with DS compared with UNet and Attention UNet without DS for temporal consistency and annulus, spline and angle errors. DS, deep supervision.

where $\mathscr{L}_{\alpha}^{(i)}$ is the ith attention coefficient map loss, computed as the binary cross-entropy between the attention coefficient map α_i and the saliency heatmap label. The saliency heatmaps were created by taking the convex hull of the segmentation labels and smoothing the edges using a Gaussian filter.

A weight scheduler allocated weights to the different loss functions such that more emphasis was given to the saliency maps at the beginning of the learning phase, and more emphasis was given to the segmentation output toward the end. The loss weight scheduler coefficient λ(n) is defined as

$$\lambda(n) = \begin{cases} 0 & \text{if } n \leq N_0 \\ \dfrac{n - N_0}{N_1 - N_0} & \text{if } N_0 < n < N_1 \\ 1 & \text{if } n \geq N_1 \end{cases} \tag{3}$$

where n is the epoch number. The constants N_0 and N_1 were set to 40 and 200, respectively.

Biomarkers for MV disease

After segmentation of the MV, we extracted biomarkers for MV morphology and motion, namely, leaflet angle, leaflet tenting area and leaflet angular velocity. These quantitative predictors correspond to biomarkers described in previous research [7–9], but are extracted automatically. The biomarker extraction is illustrated in Figure 4.

The leaflet angle ϕ is computed as

$$\phi = \arcsin(\mathbf{l} \times \mathbf{b}) \tag{4}$$

where l is the hinge-to-leaflet centroid vector and **b** is the annular plane vector, defined by the two annulus hinge points. The leaflet tenting area is computed by extracting the center curve spline **c** of the leaflet segmentation mask and computing the signed area T between **c** and **b**. The parts where **c** lies below **b** negatively affect the total area. The leaflet angular momentum is computed as the time derivative $d\phi/dt$ of the leaflet angle. Angular velocity is converted to meters/second by multiplying by the length $|\mathbf{l}|$ between the hinge point and the leaflet centroid.

Model training and evaluation

We trained and compared UNet, Attention UNet and Attention UNet + DS on the annotated data. The images were reshaped into 256 × 256 pixels. Annulus hinge points were converted into Gaussian heatmaps with a full-width half-maximum of 10 pixels. The networks were trained for 500 epochs, using the Adam optimizer with an initial learning rate of 5×10^{-4} and a batch size of 64. We used balanced cross-entropy segmentation loss (1) for all models. We applied gamma augmentation to the images with random gamma values between 0.4 and 1.7 to handle varying image contrast.

All models were trained on the same 70% of the annotated participants and tested on the remaining 30%. Moreover, we also performed the same experiment with 30% training data and 70% testing data. During testing, we evaluated standard segmentation metrics and the accuracy of leaflet angle estimation, annulus point placement and leaflet center curve spline estimation (12-point cubic splines). Additionally, we assessed segmentation quality throughout every frame in each recording by calculating a temporal consistency score, TSC(n), for each frame $\hat{y}(n)$, defined as

$$\text{TCS}(n) = \begin{cases} 1, & \text{if } \hat{y}(n) \text{ is consistent} \\ 0, & \text{otherwise} \end{cases}$$

where $\hat{y}(n)$ is considered consistent if the following conditions are met:

- Both annulus hinge points are segmented.
- None of the annulus hinge points have moved from the previous frame with a velocity higher than 0.35 m/s.
- None of the leaflets have a velocity higher than 1.5 m/s.

The annulus velocity threshold was set above twice the highest expected velocity in healthy individuals [24]. Similarly, the leaflet velocity threshold was chosen based on measured velocities in healthy individuals, which never exceeded 0.75 m/s in our data sets.

Clinical feasibility

The proposed method was applied retrospectively to three TTE exams of healthy references with no VHD, three exams of patients with MV prolapse and three exams of patients with MV stenosis. MV motion and morphology biomarkers for each leaflet scallop were extracted from representative recordings in each exam. The extracted quantitative measurements were compared with the qualitative descriptions of the MV condition in the cardiologist's report. In addition, we applied the proposed leaflet angle tracking to one healthy reference and one patient with restrictive filling of the left ventricle. The tracking results were compared qualitatively with pulsed wave Doppler spectra of MV inflow from the same exams.

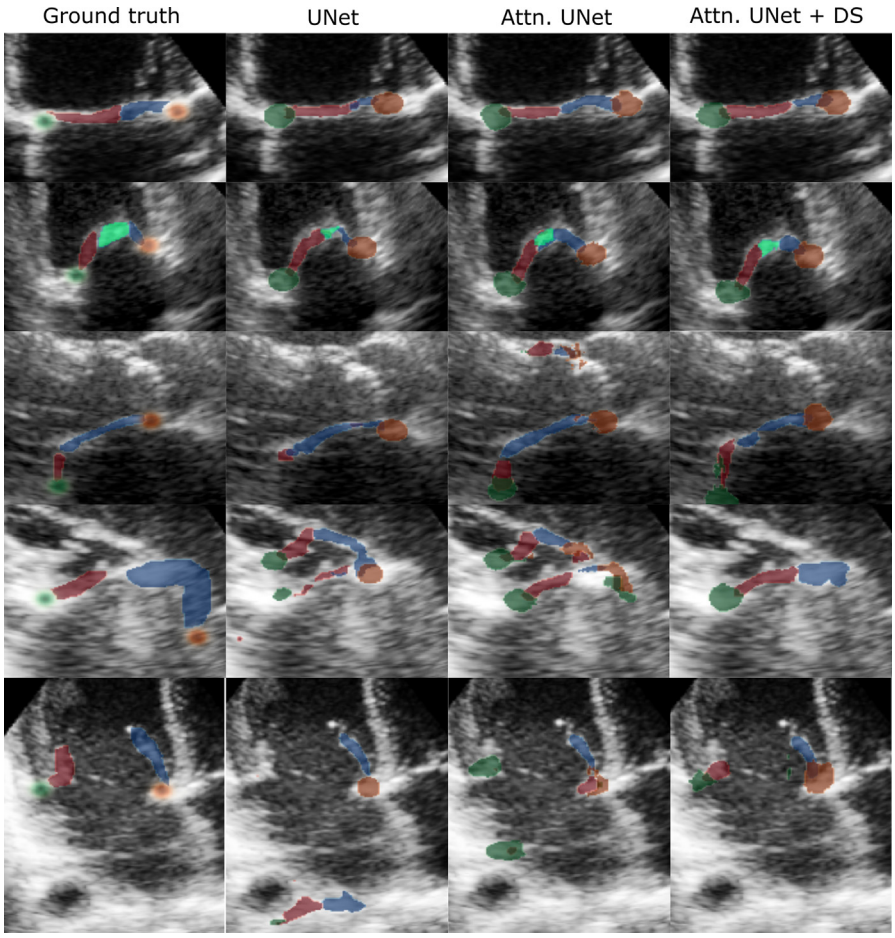

Figure 6. Segmentation examples (zoomed) from the test set (70%/30% train/test split). Attention UNet + DS mitigates false positives of other valves and tissue in the bottom three examples. Note that the bottommost example is an offset apical long-axis view where UNet failed considerably, whereas Attention UNet + DS provided reasonable results. This example indicates that Attention UNet + DS might be more robust in the presence of suboptimal views, which is a common occurrence in the clinic. DS, deep supervision.

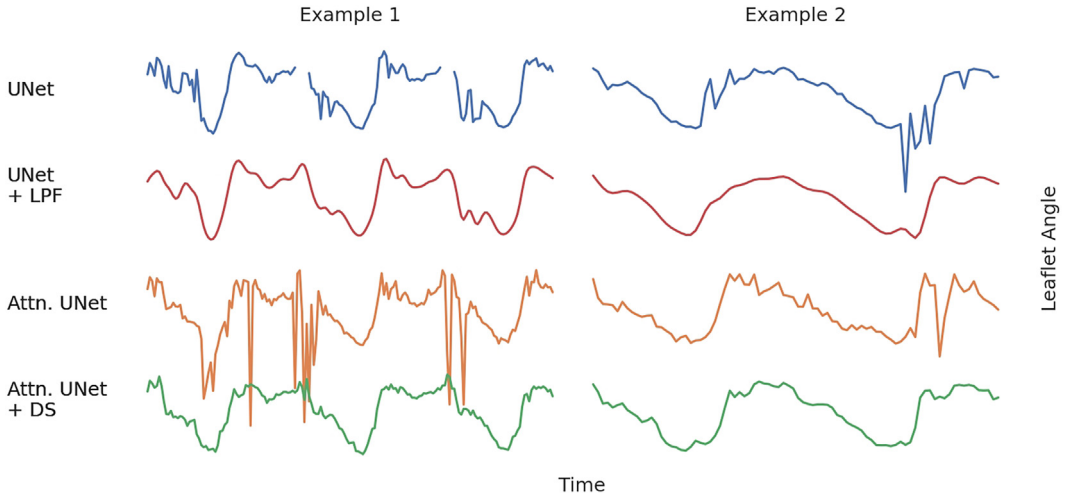

Figure 7. Leaflet angle tracking plots of two examples. In these examples, Attention UNet + DS had the highest temporal consistency and provided smoother tracking with fewer errors than the other models. Smoothing could also be achieved by LPF of the tracking result; however, this could affect accuracy and is limited to offline post-processing. DS, deep supervision; LPF, low pass filtering.

Results

Segmentation validation

Evaluation results are reported in Table 1. Key metrics are also illustrated in Figure 5. Attention UNet without DS performed notably worse than the others. Attention UNet with DS performed similarly to UNet on average; however, robustness, temporal consistency and biomarker accuracy were improved. Moreover, Attention UNet with DS significantly improved all metrics when using a 30%/70% train/test split. Figure 6 illustrates how UNet was prone to produce significant outliers in edge cases, which were mitigated using attention gates and DS. Figure 7 illustrates how attention improved temporal consistency as more coherent biomarker tracking results with fewer errors were derived.

For the Attention UNets, we can observe significant improvement when applying DS. Without DS, predictions had a relatively high error, especially regarding angle, annulus displacement and Hausdorff. Figure 8 illustrates that without applying DS, the attention coefficient maps did not necessarily emphasize only the relevant features. Consequently, as illustrated in Figure 6, Attention UNet without DS was prone to false positives in irrelevant regions. However, such false positives were mitigated using DS.

Biomarker feasibility

We evaluated the automatically extracted biomarkers for VHD on three patients with MV prolapse, three patients with MV stenosis and three healthy references. We here used the Attention UNet with DS to perform segmentation. Figure 9 shows heatmaps illustrating predicted biomarkers in the different MV scallops. These were created by combining segmentation results with view and timing classification from multiple recordings of the same participant. The results indicated that negative systolic angle and tenting area were associated with MV prolapse. Similarly, reduced leaflet movement was associated with stenosis.

MV motion and cardiac function

In addition to aiding the assessment of VHD, MV motion patterns might relate to other aspects of cardiac function, for instance, MV inflow patterns, as illustrated in Figure 10. MV motion could provide additional information on flow and pressures, which, unlike Doppler measurements, is independent of insonation angle and could be measured in several views without the need for angle correction. Cardiac function is complicated; hence, the assessment might benefit from detailed measurements, which are currently infeasible but possibly achievable through automation.

Discussion

We have described a framework for segmenting the MV leaflets and annulus points in five TTE standard views. Based on the segmentation, we proposed automatic spatiotemporal biomarkers for quantifying MV morphology and motion, including leaflet angle, velocity and systolic tenting area. The advantages of improved robustness by leveraging attention gates and DS were emphasized. Finally, we determined the clinical feasibility of the aforementioned biomarkers.

Attention UNet with DS outperformed other models by focusing on relevant regions and reducing confusion from irrelevant structures with similar features. This improved robustness, biomarker accuracy and temporal consistency, despite a slight decrease in pixelwise accuracy and Dice score. Moreover, when using a lower training fraction, Attention UNet with DS exhibited significant improvements in all metrics, implying that Attention UNet with DS was more robust when exposed to a larger test set. This improvement could indicate that it converges faster toward a desirable solution during training when labeled data are scarce. The scarcity of labeled data is the main limitation when implementing deep learning models in practice as annotation is a substantial workload for clinicians.

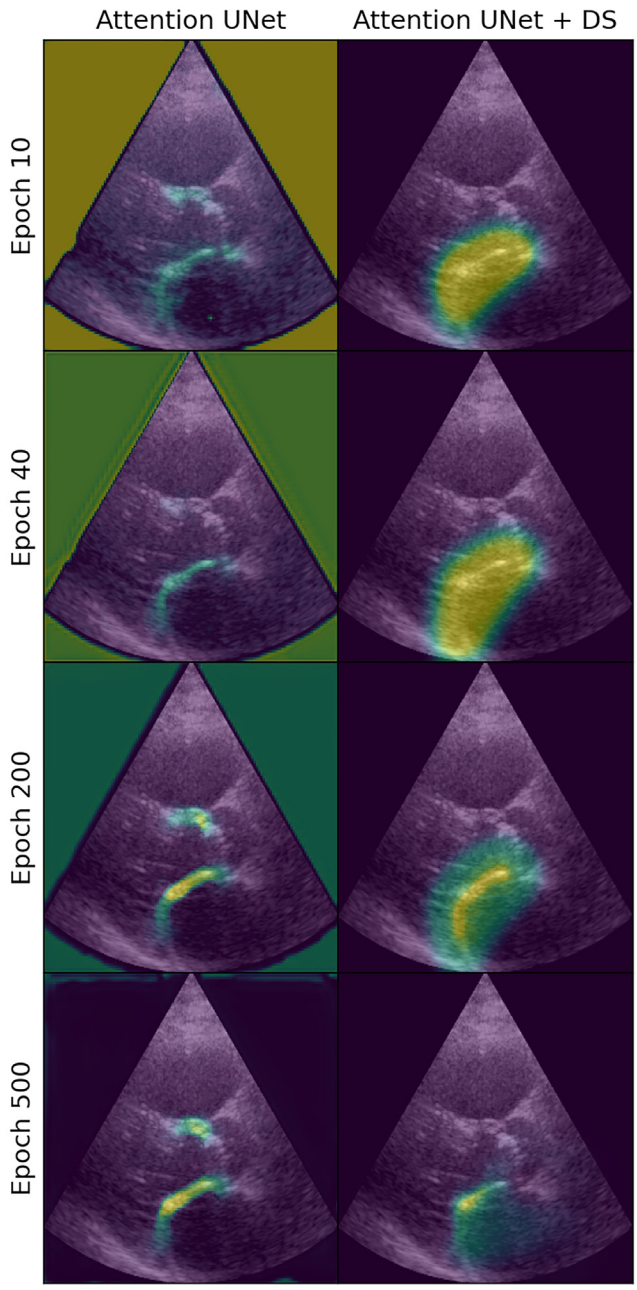

Figure 8. Evolution of the attention coefficient map α_5 during training for Attention UNet with and without DS applied. With DS, the attention coefficient maps quickly converge to emphasize the relevant region in the image. Between epochs 40 and 200, the loss weight scheduler gradually introduced the segmentation loss into the loss function. Beyond epoch 200, only the segmentation loss was optimized. We can observe that the salient region was then narrowed further toward the contour of the MV. By contrast, Attention UNet without DS highlighted both the mitral and aortic valves, proving less aligned with the desired objective. DS, deep supervision.

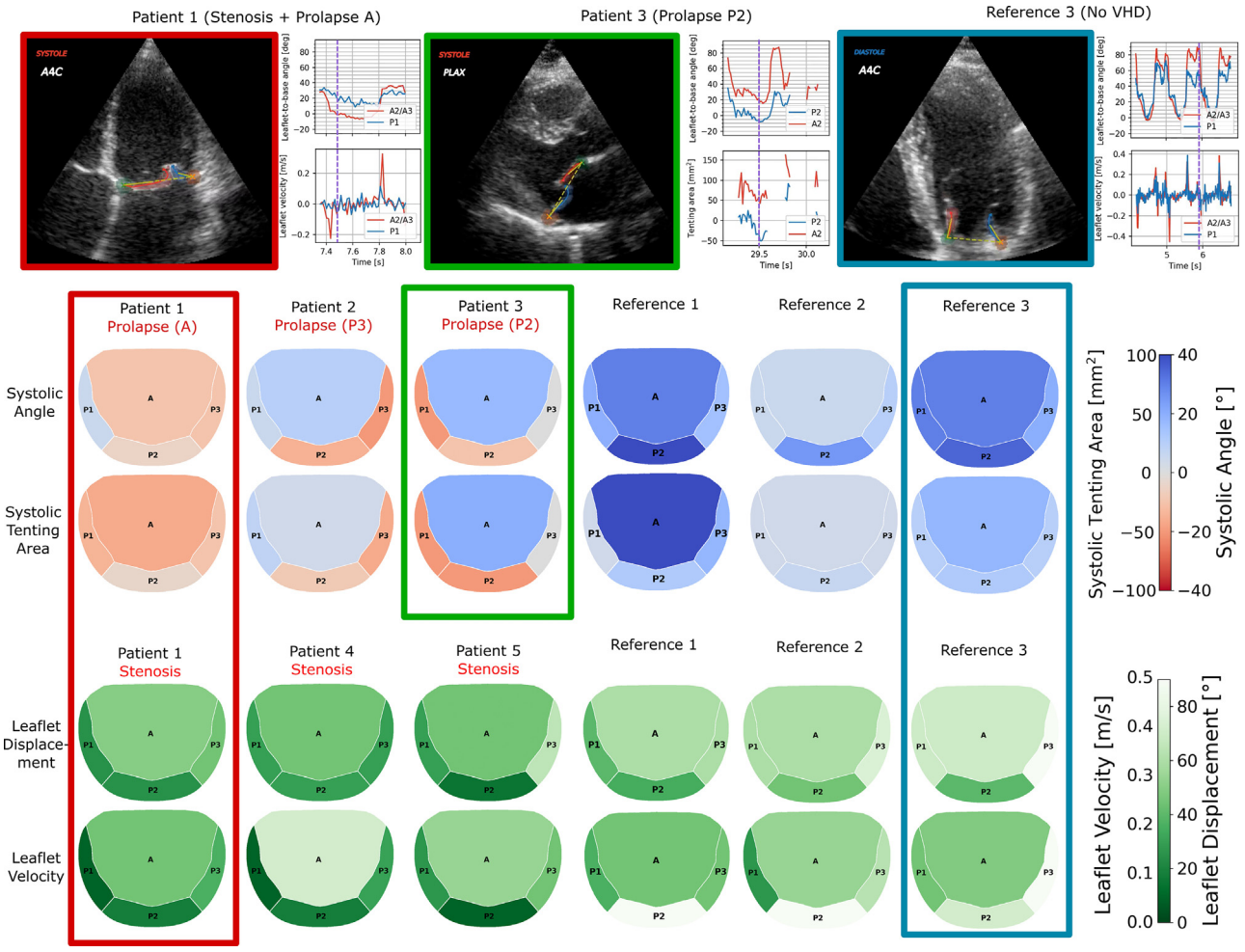

Figure 9. Top: Examples of MV segmentation, tracking and biomarker extraction for cases of stenosis, prolapse and a healthy reference. Bottom: Heatmaps of the MV (A, anterior; P, posterior; 1, anterolateral; 2, central; 3, posteromedial) revealing systolic tenting area, systolic angle, leaflet displacement and velocity measured by applying our approach on exams consisting of multiple standard echocardiogram recordings. Patients 1–3 had mitral valve prolapse at the time of the recording. According to the cardiologist's report, the scallops subject to prolapse are denoted in *red text*. Patients 1, 4 and 5 had mitral stenosis. References 1–3 were healthy individuals with no VHD. MV, mitral valve; VHD, valvular heart disease.

Traditional metrics for segmentation performance are of limited use for the MV because of its small leaflet area relative to its contour. When evaluating leaflet angles, annulus placement and center curve splines, our approach significantly improved compared with the baseline. Most notably, we observed a reduction in outliers in these metrics. This reduction can be explained by an increased robustness to out-of-domain cases, for which UNet was prone to significant failure. Such failure cases can be detected by user supervision; however, mitigating failure cases is imperative for building trust among users.

Despite satisfactory results, challenges exist for MV segmentation, especially when subject to poor image quality or when leaflets are partially visible or overlap. In poor-quality images the MV is sometimes barely visible. These cases pose challenges to the annotators, leading to higher uncertainty in the reference annotations. There was also increased uncertainty in the reference annotations for cases of severe rheumatic valve thickening, which made the model prone to flickering segmentation contours in such cases. Moreover, echocardiography is intrinsically a spatiotemporal modality, and MV leaflet motion is highly dynamic. Therefore, we believe leveraging temporal information during training is likely beneficial for improving segmentation accuracy and robustness. Similar to previous research [25–27], this might be achievable using semisupervised learning with spatiotemporal pseudo-labels.

Moreover, the MV structure might be better modeled as a graph using a graph convolutional neural network (GCN) [28]. We also expect further improvement if separate models are trained for each view, as suggested by previous research [14]. However, this requires an increased training set for all models to learn effectively.

Automatic measurements of the MV from standard echocardiograms offer benefits such as facilitating standardized assessments, reducing clinic workload and aiding non-expert users with improved visualization and detection of abnormalities. Because manual tracking of MV leaflet motion is infeasible, there is limited knowledge on how MV leaflet motion relates to VHD and heart function. Future studies will assess the clinical viability of our approach and, if possible, determine cutoff values for the proposed biomarkers. Future work should also further investigate the use of MV motion time series concerning cardiac function. We believe that studying MV leaflet motion at the various stages of diastolic dysfunction might uncover important information on interpreting the observed patterns.

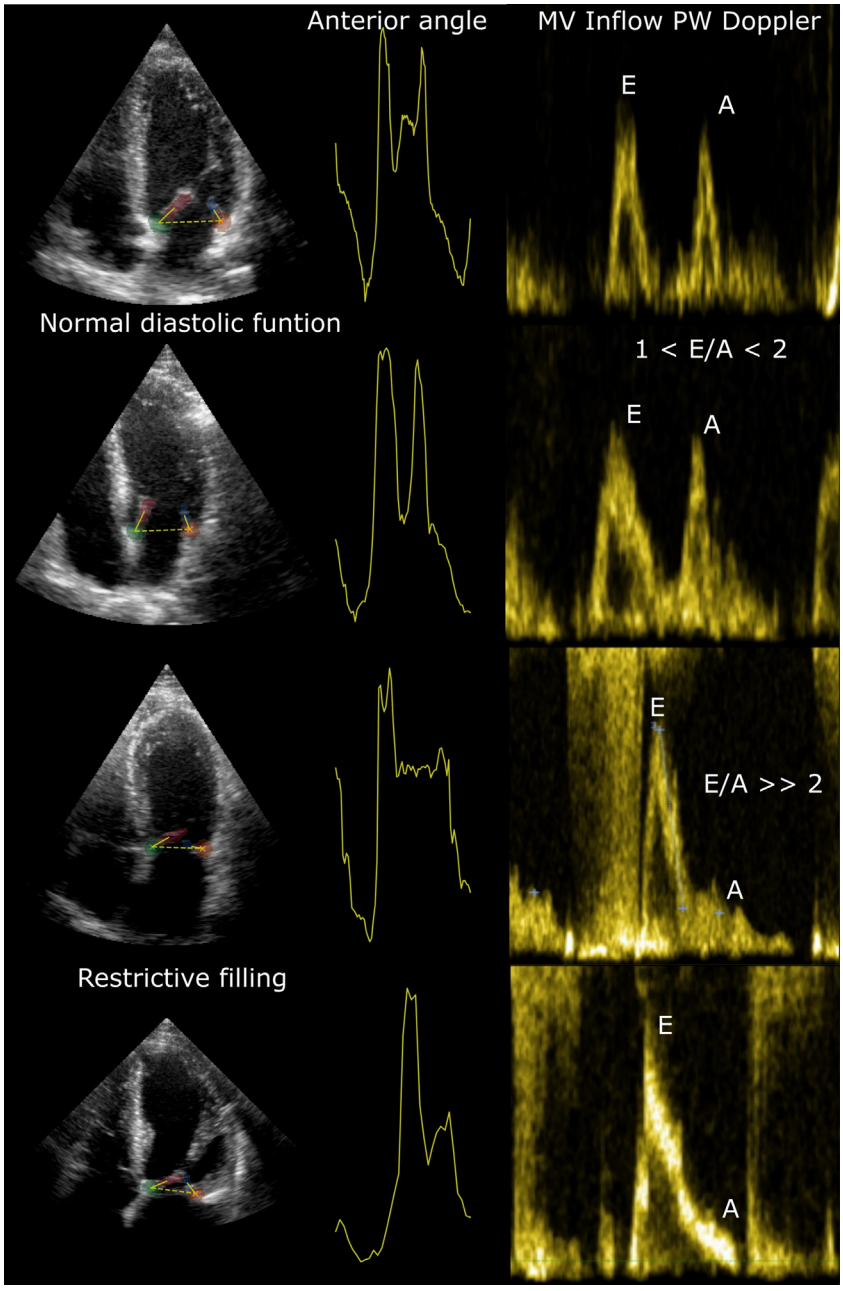

Figure 10. Tracking patterns of the anterior leaflet for A4C views in two cases of normal diastolic function (top) and two cases of restrictive filling (bottom). The tracking results (middle) are compared with MV Inflow Doppler spectra (right). We can observe that in cases of restrictive filling, the atrial systole peak angle is notably reduced, similar to the A wave velocity peak in the Doppler spectrum. MV, mitral valve; PW, pulsed wave.

Conclusion

In this work, we presented a deep learning framework for segmentation of the MV leaflets and annulus hinge points from transthoracic echocardiograms in five standard views. Moreover, we derived robust quantitative measures of angular movement and tenting areas for the different leaflet scallops, which were feasible for assessing MV prolapse and stenosis. We found that Attention UNet with DS of the attention coefficients may improve focus on salient regions in the image, improving robustness and providing higher temporal consistency. We believe automated measurements of MV morphology and motion could be valuable in the assessment of MV disease and might additionally provide information on cardiac function.

Conflict of interest

The authors declare no competing interests.

Acknowledgments

This research was made possible by funding through the Centre for Innovative Ultrasound Solutions (CIUS), appointed by the Norwegian Research Council.

Data availability statement

Data may be made available on reasonable request to the authors.

Artificial intelligence technology statement

During the preparation of this work the authors used ChatGPT (OpenAI) to improve language. After using this tool/service, the authors reviewed and edited the content as needed and take full responsibility for the content of the publication.

References

[1] Nkomo VT, Gardin JM, Skelton TN, Gottdiener JS, Scott CG, Enriquez-Sarano M. Burden of valvular heart diseases: a population-based study. Lancet 2006; 368:1005–11.

[2] Otto CM, Nishimura RA, Bonow RO, Carabello BA, Erwin III JP, Gentile F, et al. 2020 ACC/AHA Guideline for the Management of Patients With Valvular Heart Disease: A Report of the American College of Cardiology/American Heart Association Joint Committee on Clinical Practice Guidelines. Circulation 2021;143:35–71.

[3] Vahanian A, Beyersdorf F, Praz F, Milojevic M, Baldus S, Bauersachs J, et al. 2021 ESC/EACTS Guidelines for the Management of Valvular Heart Disease. Eur Heart J 2022;43:561–632.

[4] Thomas N, Unsworth B, Ferenczi EA, Davies JE, Mayet J, Francis DP. Intraobserver variability in grading severity of repeated identical cases of mitral regurgitation. Am Heart J 2008;156:1089–94.

[5] Wang A, Grayburn P, Foster JA, McCulloch ML, Badhwar V, Gammie JS, et al. Practice gaps in the care of mitral valve regurgitation: insights from the American College of Cardiology Mitral Regurgitation Gap Analysis and Advisory Panel. Am Heart J 2016;172:70–9.

[6] Hagendorff A, Knebel F, Helfen A, Stbe S, Haghi D, Ruf T, et al. Echocardiographic assessment of mitral regurgitation: discussion of practical and methodologic aspects of severity quantification to improve diagnostic conclusiveness. Clin Res Cardiol 2021;110:1704–33.

[7] Silbiger JJ. Mechanistic insights into ischemic mitral regurgitation: echocardiographic and surgical implications. J Am Soc Echocardiogr 2011;24:707–19.

[8] Magne J, Pibarot P, Dagenais F, Hachicha Z, Dumesnil J, Sénéchal M. Preoperative posterior leaflet angle accurately predicts outcome after restrictive mitral valve annuloplasty for ischemic mitral regurgitation. Circulation 2007;115:782–91.

[9] Calafiore AM, Gallina S, Di Mauro M, Gaeta F, Iacò A, D'Alessandro S, et al. Mitral valve procedure in dilated cardiomyopathy: repair or replacement? Circulation 2001;71:1146–52.

[10] Snare SR, Mjølstad OC, Orderud F, Dalen H, Torp H. Automated septum thickness measurement A Kalman filter approach. Computer Methods Programs Biomed 2012;108:477–86.

[11] Sultan M, Martins N, Costa E, Veiga D, Ferreira M, Mattos S, et al. Virtual M-mode for echocardiography: a new approach for the segmentation of the anterior mitral leaflet. IEEE J Biomed Health Inform 2019;23:305–13.

[12] Corinzia L, Laumer F, Candreva A, Taramasso M, Maisano F, Buhmann JM. Neural collaborative filtering for unsupervised mitral valve segmentation in echocardiography. Artif Intell Med 2020;110:101975.

[13] Drôge H, Yuan B, Llerena R, Yen JT, Moeller M, Bertozzi AL. Mitral valve segmentation using robust nonnegative matrix factorization. J Imaging 2021;7:213.

[14] Costa E, Martins N, Sultan MS, Veiga D, Ferreira M, Mattos S, et al. Mitral valve leaflets segmentation in echocardiography using convolutional neural networks. In: 2019 IEEE 6th Portuguese Meeting on Bioengineering (ENBENG), Lisbon, Portugal. New York. IEEE; 2019. p. 1–4.

[15] Vafaeezadeh M, Behnam H, Hosseinsabet A, Gifani P. CarpNet: transformer for mitral valve disease classification in echocardiographic videos. Int J Imaging Syst Technol 2023;33:1505–14.

[16] Chen J, Li H, He G, Yao F, Lai L, Yao J, et al. Automatic 3D mitral valve leaflet segmentation and validation of quantitative measurement. Biomed Signal Process Control 2023;79:104166.

[17] Andreassen BS, Volgyes D, Samset E, Solberg AHS. Mitral annulus segmentation and anatomical orientation detection in TEE images using periodic 3D CNN. IEEE Access 2022;10:51472–86.

[18] Ivantsits M, Pfahringer B, Huellebrand M, Walczak L, Tautz L, Nemchyna O, et al. 3D mitral valve surface reconstruction from 3D TEE via graph neural networks editors. In: Camara O, Puyol-Anton E, Qin C, Sermesant M, Suinesiaputra A, Wang S, editors. Statistical Atlases and Computational Models of the Heart: Regular and CMRxMotion Challenge Papers, STACOM 2022. Lecture Notes in Computer Science Vol. 13593. Cham: Springer; 2022.

[19] Carnahan P, Moore J, Bainbridge D, Eskandari M, Chen ECS, Peters TM, et al. DeepMitral: fully automatic 3D echocardiography segmentation for patient specific mitral valve modelling editors. In: deBruijne M, Cattin P, Cotin S, Padoy N, Speidel S, Zheng Y, editors. Medical Image Computing and Computer Assisted Intervention (MICCAI) 2021, Part V. Lecture Notes in Computer Science Vol. 12905. Cham: Springer; 2021. p. 459–68.

[20] Fiorito AM, Østvik A, Smistad E, Leclerc S, Bernard O, Lovstakken L. Detection of cardiac events in echocardiography using 3D convolutional recurrent neural networks. Proc IEEE Int Ultrason Symp 2018:1–4.

[21] Østvik A, Smistad E, Aase SA, Haugen BO, Lovstakken L. Real-time standard view classification in transthoracic echocardiography using convolutional neural networks. Ultrasound Med Biol 2019;45:374–84.

[22] Smistad E, Østvik A, Løvstakken L. Annotation Web—an open-source Web-based annotation tool for ultrasound images. Proc IEEE Int Ultrason Symp 2021:1–4.

[23] Schlemper J, Oktay O, Schaap M, Heinrich M, Kainz B, Glocker B, et al. Attention gated networks: learning to leverage salient regions in medical images. Med Image Anal 2019;53:197–207.

[24] Grue JF, Storve S, Støylen A, Torp H, Haugen BO, Mølmen HE, et al. Normal ranges for automatic measurements of tissue Doppler indices of mitral annular motion by echocardiography. Data from the HUNT3 Study. Echocardiography 2019;36:1646–55.

[25] Wei H, Cao H, Cao Y, Zhou Y, Xue W, Ni D, et al. Temporal-consistent segmentation of echocardiography with co-learning from appearance and shape. Medical Image Computing and Computer Assisted Intervention—MICCAI 2020. Cham: Springer; 2020. p. 623–32.

[26] Hu J, Smistad E, Salte IM, Dalen H, Lovstakken L. Exploiting temporal information in echocardiography for improved image segmentation. Proc IEEE Int Ultrason Symp 2022:1–4.

[27] Ling HJ, Painchaud N, Courand PY, Jodoin PM, Garcia D, Bernard O. Extraction of volumetric indices from echocardiography: which deep learning solution for clinical use? editors. In: Bernard O, Clarysse P, Duchateau N, Ohayon J, Viallon M, editors. Functional Imaging and Modeling of the Heart. FIMH 2023. Lecture Notes in Computer Science Vol. 13958. Cham: Springer; 2023.

[28] Thomas S, Gilbert A, Ben-Yosef G. Light-weight Spatio-temporal graphs for segmentation and ejection fraction prediction in cardiac ultrasound. Medical Image Computing and Computer Assisted Intervention—MICCAI 2022. Cham: Springer; 2022. p. 380–90.